Range Feature Extraction during Active Sensor Motion

N. E. Pears
Department of Engineering
Cambridge University
Cambridge, CB2 1PZ, UK
email: nep@eng.cam.ac.uk

Abstract

An active range sensor is summarised. This sensor can direct its field of view in order to fixate on range features for mobile robot navigation. The image position sensor used has a Gaussian noise characteristic with measurable variance, which makes the sensor particularly amenable to stochastic range feature detection. A geometric analysis of the sensor allows a mathematical model of the sensor to be built, the parameters of which can be determined from data collected during the calibration of the real sensor. This model forms the basis of a sensor simulation, which allows allows feature extraction algorithms to be developed. One such algorithm, based on the Extended Kalman Filter, extracts a piecewise-linear range representation of the local environment. This has a number of advantages over previous methods in that it is computationally efficient, it deals with noise appropriately, and it is robust to sensor head movements as range measurements are being made.

1 Introduction

Many different means of range sensing have been investigated for Robotics applications. These include optical radar [4], sonar, projected stripe and projected pattern [2] schemes. The latter two are based on optical triangulation which provides an effective solution for short to medium range ranging applications. An intelligent active range sensor, based on optical triangulation has been designed to guide obstacle avoidance and docking manœuvres of a mobile robot. The mechatronic design of the sensor, its calibration, its means of range variance estimation, and its local processing structure have been presented in a previous paper [5]. This paper briefly reiterates the structure of the sensor and then goes on to describe how the sensor may be modelled geometrically. This model forms the basis of a sensor simulation which models many physical properties of the ranging process. The form of the noise contaminated range scan that it generates is almost identical to that produced by the real sensor and so it provides an useful tool with which to develop range feature extraction algorithms. Section 4 describes a simple feature extraction algorithm, where the features are simply straight line segments extracted from the scan. Accurate range feature extraction is important for robust control of both the active sensing process itself and of vehicle manœuvres.

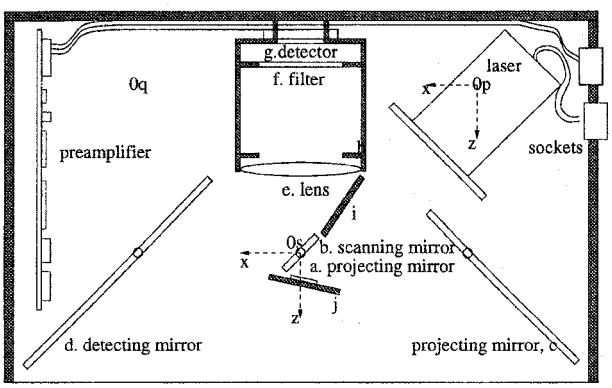

Figure 1: Plan view of the sensor head

The recursive line extraction algorithm presented here is suitable for any range sensor which provides noisy range measurements at deterministic orientations. In addition it permits (i.e. is robust to) rotations of that sensor's body (for active sensing) and does not require axes of body rotation and laser projection to be coincident.

2 The sensor configuration

This section provides a brief summary of the sensor configuration presented in [5]. The means of scanning the laser and lens in exact synchronism is shown in plan view in fig. 1, which is an adaptation of Livingstone and Rioux's [8] configuration. The laser is scanned over twice the angle over which the scanning mirror deflects, and the centre of scanning is at the virtual image point O_p. The lens is effectively scanned, in exact synchronism with the laser, around virtual image point Oq in the sensor on an arc with radius equal to the separation between the scanning mirror and the lens. The synchronised scanning optics in fig 1 is termed the *sensor head.* This sensor head is mounted on a servo driven platform which can rotate the field of view of the sensor head between +90 and -90 degrees relative to the forward looking direction.

2.1 Image position measurement

The geometric means of range measurement described above requires the one-dimensional measurement of image position. An analogue means of mea-

Proc. IROS 97 0-7803-4119-8/97/$10©1997 IEEE

surement is provided by the lateral-effect photodiode (LEP) which acts as a photocurrent divider so that the position of the light centroid, p, is

$$p = \frac{I_1 - I_2}{I_1 + I_2}\left(\frac{P}{2}\right), \qquad \left\{-\frac{P}{2} \leq p \leq +\frac{P}{2}\right\} \quad (1)$$

and the detector current, I_0, is the sum of the terminal currents, I_1 and I_2. If image position variance can be computed, it can be scaled by (the square of) the triangulation gain, which is the magnitude of the local gradient, $|\frac{\partial z}{\partial p}|_{z,\theta}$ in the calibration table to give an estimate of range variance. This variance information is essential to allow robust algorithms to be applied to the raw range data; in particular, it is used in the EKF algorithm for line segment extraction. A previous analysis [5] established a relationship between the standard deviation associated with an image position measurement and the detector current for that measurement as

$$\Delta p_n = \frac{\Delta p}{\left(\frac{P}{2}\right)} = \frac{I_n}{I_0} \quad (2)$$

In order to estimate the constant noise current, I_n, the above equation can be linearised by taking logarithms and the results in table 2 can be used to estimate the constant noise current, I_n, by standard least squares methods. This value is then used in the sensor simulation.

2.2 Sensor performance

Table 1 summarises the specifications of the sensor head and sensor head drive. Standard deviations of range measurements, and their values as a percentage of the target range, are shown in table 2. In addition, the standard deviation of image position and the average detector current in nanoamps are shown. These results are almost entirely immune to the effects of ambient lighting as laser modulation and lock-in detection are used in the sensor design [7].

Table 1. Sensor specifications

Specification	value
field of view	40 degrees
depth of field	2.1m
stand of distance (min. range)	0.4m
maximum range	2.5m
range measurements per scan	256
range measurement frequency	2.5kHz
bandwidth of detector	1kHz
scan frequency	9.8Hz
laser power	0.9mW
laser wavelength	670nm
laser class	II (max 1mW)
sensor head position resolution	0.36 degree
head response time (90 deg. step)	0.5s

Table 2. Ranging Results (1000 readings)

z(m)	σ_z(cm)	% rep.	I_o (nA)	$\Delta p(\mu m)$
0.75	0.05	0.067	48.0	3.81
1.0	0.148	0.148	26.0	6.615
1.25	0.463	0.37	16.0	11.3
1.5	0.798	0.532	11.0	15.745
1.75	1.568	1.1	8.3	22.095
2.0	2.547	1.27	6.4	29.265
2.25	3.713	1.65	5.0	35.28
2.5	7.662	3.06	4.3	45.07

3 Development of a sensor simulation

A geometric analysis of the sensor allows a model of the sensing process to be built, which can be used to form the basis of a simulation tool. This is necessary for developing and investigating feature extraction algorithms and provides a means of comparing predicted ranging performance with actual ranging performance. In the following section, the geometry of the ranging process is analysed. In section 3.2 it is shown how the parameters in this model can be derived from the calibration data of the real sensor. Finally, in section 3.3 the simulation tool which uses this model is described.

3.1 Analysis of the ranging geometry

Figure 2 is a schematic diagram of the ranging geometry in which the range of the object is assumed to be large compared with the focal length of the collecting lens so that the focal plane is at a distance f from the principal point of the lens. Essentially, the schematic is an optical ray diagram of fig. 1 with the laser projection axis and lens optical axis "unfolded" into their virtual image positions so that they rotate in synchronism about the origin $0p$ and the point q respectively. (These points correspond to the virtual positions $0p$ and $0q$ on fig. 1). Note that the centre of the lens does not coincide with the point q but rotates about q on an arc with radius s, the scanning mirror-lens separation.

In the geometric analysis of the ranging process, it is assumed that the optical centre of the lens is scanned about a point, q, which is at the same z coordinate as the origin of the laser scan, $0p$, as shown in fig. 2. The sensor was designed so that this would be the case to a good approximation.

The small angle γ in fig. 2 is required to ensure that the whole detector length is used in covering the sensor's depth of field. (This vergence angle of the optical axis should not be confused with that of the laser beam, which is the *projected* vergence angle, γ^p.)

Examination of fig. 2 reveals the following three relationships

$$\frac{x^p - d + a}{z^p} = \tan(\theta^p - \phi - \gamma) \quad (3)$$

$$\tan\theta^p = \frac{x^p}{z^p} \quad (4)$$

$$\tan\phi = \frac{p}{f} \quad (5)$$

Using these relationships we can derive the projection frame coordinates of a scene point as [6]

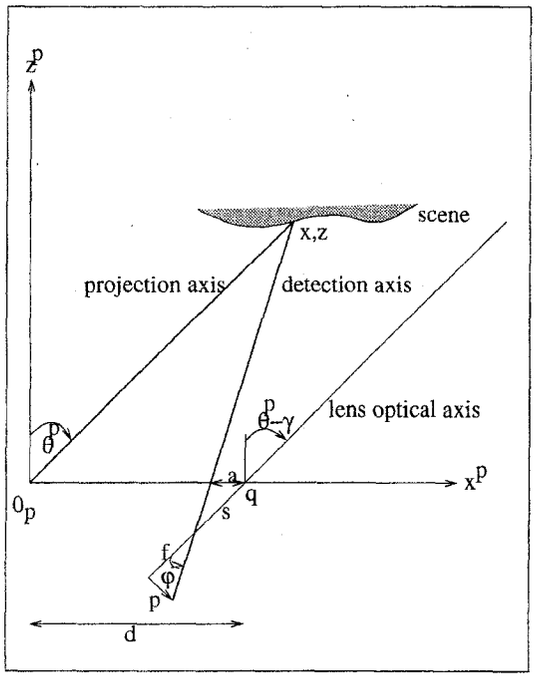

Figure 2: Projection frame geometry of ranging

$$z^p = \frac{1}{q}\mathbf{A}\mathbf{\Gamma}^T \qquad x^p = z^p \tan\theta^p \tag{6}$$

where

$$\mathbf{A} = \left[\frac{fd}{p}cos^2\theta^p, \frac{d}{2}sin2\theta^p, -scos\theta^p\right] \tag{7}$$

$$\mathbf{\Gamma} = \left[1 + (\tan\theta^p - \frac{p}{f})\tan\gamma, 1, \sec\gamma\right] \tag{8}$$

$$q = 1 + \frac{f}{p}\tan\gamma \tag{9}$$

(The superscript p refers to projection frame coordinates. A superscript s refers to sensor frame coordinates where the sensor frame has its origin on the axis of sensor head rotation). Note that the terms in Γ represent the effect of the vergence angle, since if γ were zero, then each of the terms in Γ (and q) would be unity.

3.2 Estimation of Sensor Parameters

For the sensor simulation to be a useful predictive tool, appropriate values for parameters in the geometric model must be derived. This is achieved by processing the data collected in the calibration of the real sensor. Projected vergence angle γ^p, and the origin of the sensor scan $[x^s_{0p}, z^s_{0p}]^T$ are given to the simulation directly from the x calibration phase which uses a striped target [6]. This leaves parameters f, d, γ, s to be determined from the z calibration table which contains values of image position for 256 angles by approximately 40 calibration target depths.

Equation 6(a) can be rearranged to give

$$p = \frac{f(z^p\tan\gamma - d\cos^2\theta^p(1+\tan\theta^p\tan\gamma))}{d\cos\theta^p(\sin\theta^p - \cos\theta^p\tan\gamma) - s\cos\theta^p\sec\gamma - z^p} \tag{10}$$

Substituting $(z^s - z^s_{0p})$ for z^p in the above gives

$$p(z^s - z^s_{0p}) = \mathbf{H}\mathbf{x} \tag{11}$$

where

$$\mathbf{H}^T = \begin{bmatrix} p\cos\theta^p\sin\theta^p_s \\ -p\cos^2\theta^p_s \\ -p\cos\theta^p_s \\ \cos^2\theta^p_s \\ \sin\theta^p_s\cos\theta^p_s \\ z^s_{0p} - z_s \end{bmatrix} \tag{12}$$

$$\mathbf{x} = \begin{bmatrix} d \\ d\tan\gamma \\ s\sec\gamma \\ fd \\ fd\tan\gamma \\ f\tan\gamma \end{bmatrix} \tag{13}$$

Equation 11 illustrates that determining the sensor's four intrinsic parameters involves determining the state $\mathbf{x}$, which has dimension 6. The data forming the calibration look-up table typically will contain 10240 data points, thus enabling an accurate LS solution to be formed for $\mathbf{x}$ in equation 11.

3.3 The sensor simulation tool

In the sensor the laser beam has a width of around 3mm, and this is modelled as a number of parallel rays (typically 9) spanning this width. The intensity of these rays is such that they sum to the power of the laser beam, with the rays at the edge being less intense than at the centre. (The rays effectively sample the Gaussian distribution of intensity across the beam width.) The world is modelled as a series of line segments, each with an associated reflectivity and the sensor simulation takes the following form:

- The results of both stages of the calibration are passed to the simulation. Using these results, the approach described in section 3.2 allows the sensor intrinsic parameters to be estimated. When these values are placed into the equation 6 they form a geometric model.

The following steps take place for each of the 256 projection angles.

- The nearest intersection of each ray with the environment is computed. Rays, environment segments, and points of intersection are represented in homogenous coordinates to simplify computations to cross products.

- For each ray, an image position is computed using the geometric model. Some points of intersection may be occluded from the image sensor by another part of the environment (missing parts) and, in this case, the computation is not performed.
- For each ray, its contribution to the total detector current is determined. (Occluded rays have zero contribution.) This is dependent on the ray's projection intensity, the range from the lens at which it intersects the environment, and the reflectivity of the environment at that intersection point.
- The image position formed by the whole laser projection is the weighted sum of the image positions due to each ray. The weights are the proportion of the ray's contribution to the total detector current. (This models the integration of image intensity over the surface of the detector).
- The detector current is the sum of all the detector currents generated by each ray.
- Total detector current is used to compute the image position variance from equation 2. (The current noise figure, I_n must computed from an off line experiment with the real sensor using standard LS on logarithmic plots). Image position noise is added by pseudo-randomly sampling from a zero mean Gaussian distribution with this variance.
- $[x^s, z^s]^T$ can then be determined in the same way as the actual sensor by interpolating using the real calibration table for z_s, and using the scan origin and projection vergence parameters identified from the sensor x calibration to generate x_s.
- The position measurements and their variances can be passed to a line extraction EKF algorithm which can subsequently be used on the real sensor.

4 Line extraction using the EKF

It is assumed that the range data set for a given scan can be associated with a piecewise linear model of the world. For many real environments in which autonomous vehicles operate (containing, for example, walls, pillars and boxes) this assumption is not unrealistic. Parts of the environment where the assumption does not hold can be identified because the discontinuities extracted will not exhibit predictable behaviour when the vehicle and sensor head move.

The feature extraction algorithm must estimate the parameters of the line segments, the position of range discontinuities, and their associated uncertainties. In addition, to avoid latency, a recursive formulation is required. In a recursive formulation, the choice of line segment representation is important. Some lines generated by a laser scanner [3] have employed a {midpoint, length, orientation} representation. This is not appropriate in a recursive extraction scheme because both length and midpoint are changing with each new point. A polar representation of line segments (length and orientation of line normal) does not suffer from this problem. Recent work [9] uses this representation in a method of batch orthogonal least squares on a subset (window) of measurements. A polar representation of the line segment was extracted from each window of measurements, and this process was repeated by sliding the window across the whole set of n measurements. Points were then clustered in the polar coordinates of the extracted window segments to extract line segments associated with physical features. In high scanning rate applications this approach may be a computational burden as a new batch solution has to be computed for each point. An approach which is relatively fast would be the standard formulation of a recursive LS estimator. However, this is inappropriate, since the world coordinates x and z are not independent, but are related through the laser scan angle (in fact x needs to be deterministic). Also this formulation does not provide a framework with which to deal with rotations of the sensor body. This is important because such rotations can be significant in the time it takes for a single scan (0.1s). In addition to being a stable representation in a recursive feature extraction scheme, a polar representation (bounded by scan angles) is appropriate for dealing with sensor head rotations in the Extended Kalman Filter (EKF). This provides the computational framework in which sensor head movements are catered for by the evolution of such a state representation.

4.1 State prediction

In the (Extended) Kalman Filter, a process (or plant) model describes how the state, $\mathbf{x}$, evolves with an input vector, $\mathbf{u}$, subject to an additive noise vector, $\mathbf{v}$. This model has the general form [1]:

$$\mathbf{x}(k+1) = \mathbf{f}(\mathbf{x}(k), \mathbf{u}(k)) + \mathbf{v}(k), \quad \mathbf{v}(k) \sim N(\mathbf{0}, \mathbf{Q}(\mathbf{k})) \tag{14}$$

where $\mathbf{f}$ is the state transition function, and the notation $\mathbf{v}(k) \sim N(\mathbf{0}, \mathbf{Q}(\mathbf{k}))$ denotes that the noise source is modelled as zero-mean Gaussian with covariance $\mathbf{Q}(k)$.

The process in the line extraction EKF is the rotation of the sensor head and, in the process model, the state representation of the current line segment must evolve appropriately. The geometry of fig. 3 representing time sample k gives

$$\rho^p(k) = \rho^s(k) + r_0 \cos\beta(k) \tag{15}$$

where

$$\beta(k) = \phi^p(k) - \phi_0 \tag{16}$$

and $[r_0, \phi_0]^T$ are the projection frame polar coordinates of the sensor frame origin, derived from the calibration procedure as:

$$r_0 = \sqrt{x^{s2}_{0p} + z^{s2}_{0p}} \qquad \phi_0 = \tan^{-1}\left(\frac{z^s_{0p}}{x^s_{0p}}\right) \tag{17}$$

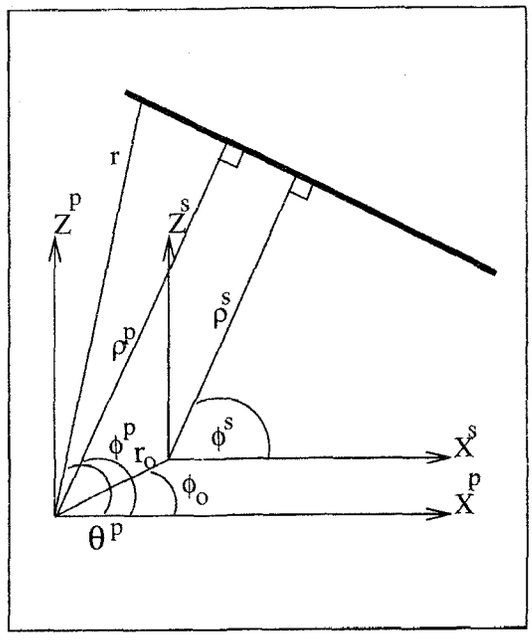

Figure 3: Polar measurement of a polar line

Now if we allow a small rotation of the sensor head, $\Delta\theta_s$, during a range sample interval, then at time interval (k+1) we have

$$\beta(k+1) = \beta(k) - \Delta\theta_s \tag{18}$$

but

$$\rho^s(k+1) = \rho^s(k) \tag{19}$$

Thus, we can combine equation 15 for time interval k and time interval $k+1$ to give the state prediction in the projection frame as:

$$\begin{bmatrix} \hat{\rho}(k+1|k) \\ \hat{\phi}(k+1|k) \end{bmatrix} = \begin{bmatrix} \hat{\rho}(k|k) + r_0(\cos\beta(k+1) - \cos\beta(k)) \\ \hat{\phi}(k|k) - \Delta\theta_s \end{bmatrix} \tag{20}$$

It is evident that the process is more natural if the state is represented in the sensor frame, since the origin of this frame is at the axis of sensor head rotation ($r_0 = 0$ in equation 20). In this case, the state prediction is linear and trivial to compute. However, since this representation yields a complex measurement equation, the state is chosen to be the polar representation of a line segment in the *projection* frame, $[\rho^p, \phi^p]^T$. The penalty is a more complex state prediction, but this is justified since the head will not always be moving when observations are being made.

4.2 Covariance of the state prediction

The covariance of the prediction is then computed as

$$\mathbf{P}(k+1|k) = \nabla\mathbf{f}\mathbf{P}(k|k)\nabla\mathbf{f}^T + \mathbf{Q}^\mathbf{P}(k) \tag{21}$$

where $\nabla\mathbf{f}$ is the Jacobian of the state transition function 14

$$\nabla\mathbf{f} = \begin{bmatrix} 1 & r_0(\sin\beta(k) - \sin\beta(k+1)) \\ 0 & 1 \end{bmatrix} \tag{22}$$

The superscript p in equation 21 indicates that any process noise must be represented in the projection frame. Process noise arises due to error in the measurement of the change in sensor head angle over a range sample interval, and may arise, for example, from the quantisation error in rotary encoders. In the implementation presented here, the velocity of the sensor head is known accurately (because of the geared stepper drive system) and thus errors in the computation of $\Delta\theta_s$ are negligible compared to range measurement errors; however we include a discussion of process noise for completeness: Any process noise due to the measurement of $\Delta\theta_s$ will appear as noise associated with ϕ_s whereas ρ_s will be unaffected, thus

$$\mathbf{Q}^s = \begin{bmatrix} 0 & 0 \\ 0 & \sigma^2 \end{bmatrix} \tag{23}$$

and this can be transformed to the projection frame as

$$\mathbf{Q}^p = \nabla\mathbf{t}\mathbf{Q}^s\nabla\mathbf{t}^T \tag{24}$$

where $\nabla\mathbf{t}$ is the Jacobian of the transform between the sensor frame state and the projection frame state

$$\nabla\mathbf{t} = \begin{bmatrix} 1 & -r_0 sin(\phi^p - \phi_0) \\ 0 & 1 \end{bmatrix} \tag{25}$$

4.3 Observation prediction

The measurement model has the form

$$r(k) = h(\mathbf{x}(k), \theta^p) + w(k), \quad w(k) \sim N(0, R(k)) \tag{26}$$

where the measurement function, $\mathbf{h}$ relates the state, the input (laser projection angle) and the observation (range), and $\mathbf{w}$ is additive, zero mean, Gaussian observation noise.

In addition to a polar state, we consider a polar formulation, (r, θ^p), of the measurement equation. The advantage of this approach is that the scan angle θ^p can be considered to be deterministic, whereas z and x are random and correlated. Thus the feature extraction EKF is based on the polar measurement of a line segment represented in polar coordinates, as depicted in fig. 3. Thus, using the geometry of this figure, the predicted state is used to generate a predicted observation as

$$\hat{r}(k+1) = h(\hat{\mathbf{x}}^p(k+1|k), \theta^p) = \frac{\rho^p}{\cos(\phi^p - \theta^p)} \tag{27}$$

4.4 Observation validation

A matching or data association procedure is required to establish whether the current observation lies on the current line segment. Such observation validation is implemented using a validation gate, which normalises the square of the difference between the actual and the predicted observation (the innovation) with the covariance of this quantity, and then tests whether it is below a threshold, g^2. Such a test indicates that the actual observation lies within g standard deviations of the predicted observation and if successful, the observation can be used to update the state estimate, otherwise the bootstrap batch processing is initialised to generate the initial state estimation of a new line segment.

The innovation is defined as the difference between the actual and the predicted observation:

$$\nu(k+1) = r(k+1) - \hat{r}(k+1|k) \tag{28}$$

The innovation covariance is obtained by linearising equation 26 about the prediction. We then square and take expectations to give, $S = E\left[\nu^2\right]$ as

$$S(k+1) = \nabla\mathbf{h}(k+1)\mathbf{P}(k+1|k)\nabla\mathbf{h}^T(k+1) + R(k+1) \tag{29}$$

where

$$\nabla\mathbf{h} = \left[\begin{array}{cc} \frac{1}{\cos(\phi^p - \theta^p)}, & \frac{\rho\tan(\phi^p-\theta^p)}{\cos(\phi^p-\theta^p)} \end{array}\right] \tag{30}$$

To generate $R(k+1) = \sigma_r^2(k+1)$, the zero mean Gaussian noise computed for z must be transformed to a noise on the measured range, whilst scan angle is considered to be deterministic. Variance in the x dimension is given by

$$\sigma_x^2 = \cot^2\theta^p\sigma_z^2 \tag{31}$$

hence

$$\sigma_r^2 = \sigma_z^2(1+\cot^2\theta^p) = \sigma_z^2 cosec^2\theta^p \tag{32}$$

Having computed the covariance of the innovation, association of the observation with the current state is achieved through a validation gate test, which is defined by

$$\frac{\nu^2(k+1)}{S} \leq g^2 \tag{33}$$

4.5 State and covariance update

The well known information form of the Kalman filter [1] is used giving the state update for validated observations as

$$\hat{\mathbf{x}}(k+1|k+1) = \hat{\mathbf{x}}(k+1|k) + \mathbf{W}(k+1)\nu(k+1) \tag{34}$$

and covariance update as

$$\mathbf{P}(k+1|k+1) = \mathbf{P}(k+1|k) - \mathbf{W}(k+1)S(k+1)\mathbf{W}^T(k+1) \tag{35}$$

where W is the Kalman gain, which is computed as

$$\mathbf{W}(k+1) = \mathbf{P}(k+1|k)\nabla\mathbf{h}^T S^{-1}(k+1) \tag{36}$$

4.6 The batch initialisation process

At the start of a range scan, and when an observation is not validated, a k point ($k \geq 2$) batch initialisation process is required to provide the initial state estimate, $\hat{\mathbf{x}}(k|k)$, and associated covariance, $\mathbf{P}(k|k)$, on which the recursive process can operate. The problem may be formulated as a non-linear least squares minimisation with $[\rho^p, \phi^p]^T$ chosen to minimise:

$$[\hat{\rho}^p, \hat{\phi}^p]^T = argmin_{\rho,\phi}\Sigma\left[r_i - \frac{\rho^p}{\cos(\phi^p - \theta_i^p)}\right]^2 \tag{37}$$

However, it is not desirable to implement an iterative solution to this equation in an algorithm which must run in real-time. A preferable approach is transform the problem into a more tractable linear form. As with the recursive process, it is inappropriate to use a batch LS estimator directly to estimate the initial state, since the world coordinates x and z are not independent, but are related by the scan angle. To minimise the projection of errors into the x coordinate, which allows a standard batch LS to be applied, the following algorithm is implemented.

Initialisation algorithm

(i) Transform measurements $[x, z]_i^p, i = 1..n-1$ to projection frame n. (This compensates for any sensor head movements during the initialisation process.)
(ii) Compute the centroid of the data set in projection frame n and determine the angle, θ_c, of the centroid with respect to the z^p axis of this frame.
(iii) Apply a rotation matrix to the n initialisation points so that the centroid is coincident with the z^p axis.
(iv) Compute a standard weighted least squares on the transformed points to give a gradient-intercept ($y = ax + b$) representation of the line segment.
(iv) Transform above representation to a polar representation $[\rho^p, \phi^p]^T$, such that

$$\phi = \tan^{-1}a - \theta_c + \frac{\pi}{2}, \quad \rho = z_m\cos(\tan^{-1}a) \tag{38}$$

(vi) Compute the covariance associated with this estimate as:

$$\mathbf{P}(k|k) = \left[\nabla\mathbf{h}^T\mathbf{R}^{-1}\nabla\mathbf{h}\right]^{-1} \tag{39}$$

In the above, $\nabla\mathbf{h}$ is the stacked Jacobian measurement matrix

$$\nabla\mathbf{h} = \left[\begin{array}{cc} \frac{1}{\cos(\phi^p-\theta_1^p)} & \frac{\rho\tan(\phi^p-\theta_1^p)}{\cos(\phi^p-\theta_0^p)} \\ \vdots & \vdots \\ \frac{1}{\cos(\phi^p-\theta_k^p)}, & \frac{\rho\tan(\phi^p-\theta_k^p)}{\cos(\phi^p-\theta_k^p)} \end{array}\right] \tag{40}$$

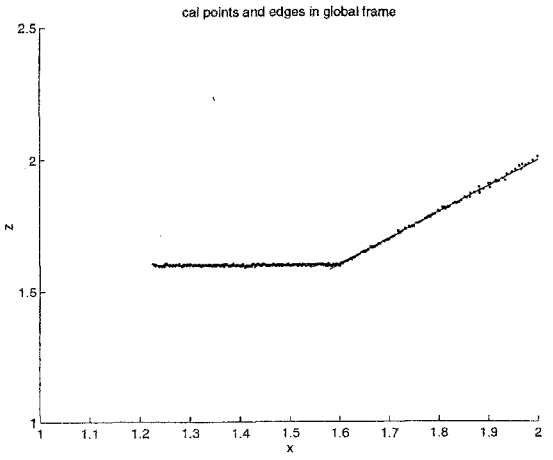

Figure 4: Sensor at x=1.5m z=0.5m

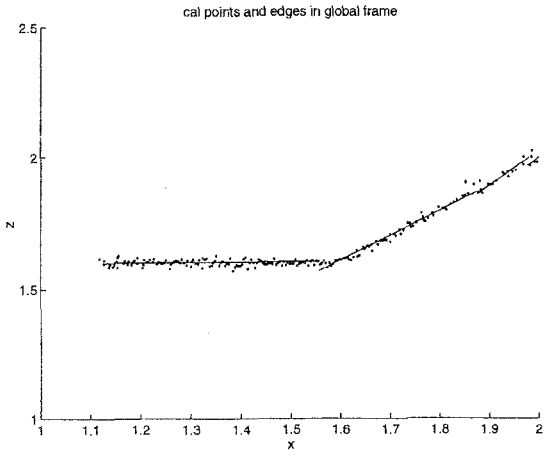

Figure 5: Sensor at x=1.5m z=0.0m

and $\mathbf{R}$ is a diagonal matrix of observation variances

4.7 Results

Figures 4 and 5 show results of the line extraction algorithm when the sensor is facing towards an edge. In the first figure, the sensor origin is positioned at (1.5,0.5) and a scan is taken. In this case the EKF algorithm generated two edges, which accurately represent the underlying structure of the environment. Figure 5 shows the range measurements and EKF output in the same environment, but with the sensor moved back to (1.5,0.0). In this case the form of the environment is still extracted but has become more fragmented. (4 segments rather than 2 are generated.) This is because the errors due to linearisation of the sensor geometry in the EKF become larger with larger deviations in range. Current work is examining approaches to solving this problem, which include clustering with weighted averaging in (ρ, ϕ) space and examining the effects of changing the threshold g.

5 Conclusions

A simulation based on a geometric model of the sensor has been developed and the range scans that it generates correlate closely with those obtained from the real sensor. This means that it is a valid and useful tool with which to develop range feature extraction algorithms. A line segment extraction algorithm has been developed which allows sensor head movements to be naturally modelled as the process in an EKF framework. In addition, this formulation avoids the problem of ill-conditioned vertical lines in a Cartesian gradient-intercept formulation. A polar measurement equation has proved to be appropriate since the dominant noise source is in range measurement rather than scan angle measurement. Also, the EKF provides variances around both the model parameters and the edge positions, making the abstracted data amenable to both tracking and probabilistic reasoning.

Ongoing work is extending these ideas by broadening the range feature types to include curved segments. This requires the correct model type to be hypothesised in the batch initialisation process.

References

[1] Bar-Shalom and Li. *Estimation and Tracking: Principles, Techniques and Software.* Artech House Inc., Boston, USA., 1993.

[2] Lo H.R. Blake A., McCowen D. and Konash D. Epipolar geometry for trinocular active range sensors. In *Proc. British Machine Vision Conf.*, 1990.

[3] P. Weckesser et al. Exploration of the environment with an active and intelligent optical sensor system. In *Proc. IEEE/RSJ Int. Conf. on Intelligent Robots and Systems*, pages 664–671, 1996.

[4] Miller G.L. and Wagner E.R. An optical rangefinder for autonomous robot cart navigation. In *SPIE 852*, pages 122–134, 1987.

[5] Pears N.E. An intelligent active range sensor for vehicle guidance. In *Proc. IEEE/RSJ Int. Conf. on Intelligent Robots and Systems*, pages 81–88, 1996.

[6] Pears N.E. An intelligent range sensor: Design, calibration and processing for mobile robot guidance. *Cambridge University Engineering Department Technical Report, CUED/F-INFENG/TR 262*, 1996.

[7] Pears N.E. and Probert P.J. An optical range sensor for mobile robot guidance. In *Proc. IEEE Int. Conf. on Robotics and Automation*, 1993.

[8] Livingstone F. R. and Rioux M. Development of a large field of view 3-d vision system. In *SPIE 665*, pages 188–194, 1986.

[9] Tschichold-Gurman N. Vestli S.J. Mops, a system for mail distribution in office type buildings. In *Proc. IEEE/RSJ Int. Conf. on Intelligent Robots and Systems*, pages 489–496, 1996.